International Conference on Space Optics—ICSO 2004

Toulouse, France

30 March–2 April 2004
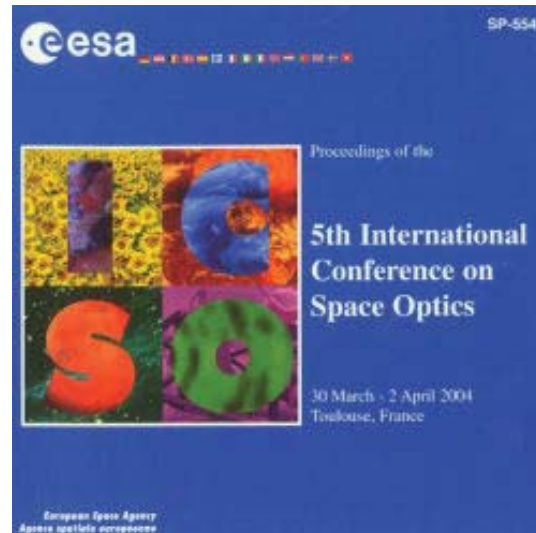
Static and dynamic micro deformable mirror characterization by phase-shifting and time-averaged interferometry

Arnaud Liotard, Frédéric Zamkotsian

STATIC AND DYNAMIC MICRO DEFORMABLE MIRROR CHARACTERIZATION BY PHASE-SHIFTING AND TIME-AVERAGED INTERFEROMETRY

Arnaud Liotard, Frédéric Zamkotsian

Laboratoire d'Astrophysique de Marseille (LAM),2,place Le Verrier,13248 Marseille Cedex 4,France

E-mail : arnaud.liotard@oamp.fr

ABSTRACT

The micro-opto-electro-mechanical systems (MOEMS), based on mature technologies of micro-electronics, are essential in the design of future astronomical instruments. One of these key-components is the micro-deformable mirror for wave-front correction. Very challenging topics like search of exo-planets could greatly benefit from this technology. Design, realization and characterization of micro-Deformable Mirrors are under way at Laboratoire d'Astrophysique de Marseille (LAM) in collaboration with Laboratoire d'Analyse et d'Architecture des Systèmes (LAAS).

In order to measure the surface shape and the deformation parameters during operation of these devices, a high-resolution Twyman-Green interferometer has been developed. Measurements have been done on a tiltable micro-mirror ($170*100\mu m^2$) designed by LAM-LAAS and realized by an American foundry, and also on an OKO deformable mirror (15mm diameter). Static characterization is made by phase shifting interferometry and dynamic measurements have been made by quantitative time-averaged interferometry. The OKO mirror has an actuator stroke of 370 ± 10nm for 150V applied and its resonant frequency is 1170 ± 50 Hz, and the tiltable mirror has a rotation cut-off frequency of 31 ± 3 kHz.

1. WAVE-FRONT CORRECTION AND MICRO DEFORMABLE MIRRORS

Diffraction-limited images rely on very efficient wave-front correction (WFC) systems. Wave fronts are affected by numerous factors such as atmosphere turbulence for ground-based telescopes, thermal deformations or optical aberrations for both ground-based and (low-cost) space telescopes. Perturbations have to be measured and corrected in real time using wave-front sensors and deformable mirrors. Up to now, these mirrors are using high-cost and large size piezo-electric actuators. For next generation WFC as Adaptive Optics for extremely large telescopes, the realisation of mirrors with several thousands actuators is needed and classical technology cannot reach this goal. Micro deformable mirrors based on MEMS technology seems to be the best challenger. Two classes of micro-

deformable mirrors have been demonstrated with the OKO mirror and the Boston Micromachines mirror.

The OKO mirror (1995) is made by bulk micromachining. A very thin 15mm-diameter reflective membrane is suspended above an array of 37 electrodes, patterned on a PCB [1]. With surface micromachining technology, Boston Micromachines has built in 2000 a $3*3mm^2$ deformable mirror, with 140 actuators with $1\mu m$ actuator stroke and a $1.5\mu m$ maximal deformation of the membrane [2]. These mirrors show good capabilities but their characteristics cannot complete the next generation WFC requirements.

Since a few years design, realization and characterization of a novel micro-Deformable Mirrors are under way at Laboratoire d'Astrophysique de Marseille (LAM) in close collaboration with Laboratoire d'Analyse et d'Architecture des Systèmes (LAAS, Toulouse, France). The characterization bench developed at LAM will make the complete analysis of these new components.

The first part of this paper presents the realization of the studied components. The second part is a description of the set-up followed by results obtained with phase-shifting interferometry. Finally, we show some dynamic results with quantitative time-averaged interferometry.

2. REALIZATION OF MICRO DEFORMABLE MIRRORS

MOEMS consists in creating a three-dimensional structure by stacking sacrificial and structural layers and using a set of masks during the deposition and the etching of these layers. New materials and new architectures are under development to reach the WFC systems requirements.

2.1. Principles

Actuation of components can be obtained by balancing spring force and electrostatic force. The spring force is dependant on the materials parameters such as Young's modulus, Poisson ratio, and on the geometric parameters of the spring. The electrostatic force F is defined by Eq. 1, where ε_0 is the vacuum permittivity, $_r$ the dielectric constant of the material in the inter-

electrode spacing, S the surface of the electrode, V the voltage applied, and d the distance between the electrode and the moving part of the component. This force is proportional to the square of the applied voltage V; therefore the force is only attractive.

$$F = \frac{\varepsilon_r \varepsilon_0 S V^2}{d^2} \qquad (1)$$

Our micro deformable mirror architecture is an array of electrostatic actuators (Fig. 1), pulling down a reflecting continuous membrane via attachment posts (Fig. 2).
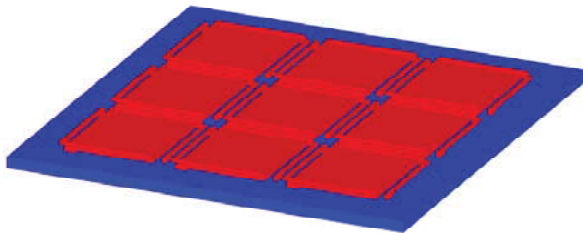

Fig. 1: Array of piston actuators

In Fig. 1 is shown an array of 3*3 piston actuators. Two spring arms link each piston plate to the substrate. In consequence the piston plates are moving down with the driving voltage. Fig. 2 is a cross-section view of the deformable mirror. Actuators and membrane are realized in the same material, and a reflective layer is coated on top of the structure.

Fig. 2: Structure of micro-deformable mirror

Requirements on deformable mirrors for next generation WFC systems are a size of actuator in the range of a few hundreds of microns to one millimetre and a stroke around ten microns.

2.2.   Results obtained at LAAS

Bricks of component have been realized with polymer materials at LAAS. A high optical quality mirror is the most challenging building block for this device. Fig. 3a represents a piston actuator before the sacrificial layer is etched. The flatness of the structural layer (500*500µm²) is very promising: 200nm P-V [3]. Fig. 3b represents a structural layer once the sacrificial

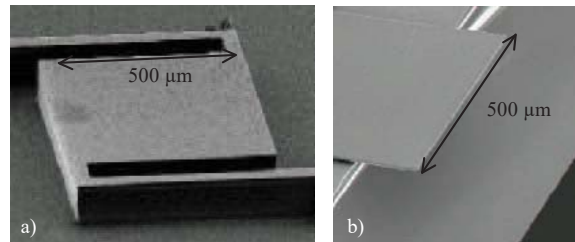layer is etched; the structure is flat without evident strain gradient.

Fig. 3: a) Actuator,   b) Structural layer

2.3.   Cronos components

A chip designed by LAAS-LAM has been realized in the American foundry Cronos. Structural layers are in poly-silicon and sacrificial layers are in silicon oxide. Two structural layers are available, but we use only the upper layer in order to have the maximum gap (2.75µm) between the electrode and the structural layer. The most representative device is the tiltable mirror shown in Fig. 4. The dimensions of the plate are 170*100µm², the torsion bar is 10µm wide. A gold reflective layer is coated on top.
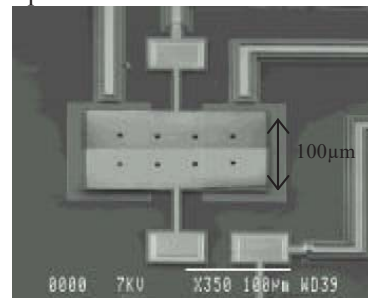

Fig. 4: SEM photo of tiltable mirror

The deposition of the 500nm-thick bottom electrodes creates a step of 500nm on the top layer. These print-through effects must be minimized for getting a high-quality mirror.
This tiltable micro-mirror can be actuated by applying a voltage between the electrodes and the mobile plate. However the stroke is limited and we must avoid any pull-in of the plate on the substrate. Usually, take-off is obtained by decreasing the voltage, but a long contact could lead to a definitive sticking due to charge accumulation.

Characterization of MOEMS is complex because these devices need to be analysed optically, mechanically and electronically. Moreover MOEMS are systems where all parts are interacting. And finally their small size increases the complexity of their characterization.

3. INTEROMETRIC CHARACTERIZATION BENCH

An interferometric characterization bench has been developed in order to measure the shape and the deformation parameters of these devices. All the optical characterizations in a static or dynamic behaviour are performed including optical surface quality at different scale, actuators stroke, maximum mirror deformation and cut-off frequency.

3.1. Description

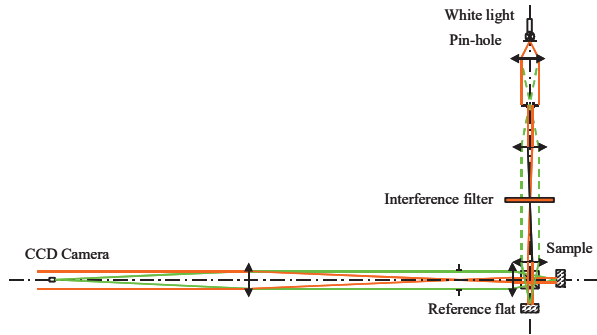This bench is a high-resolution and low-coherence Twyman-Green interferometer (Fig. 5).

White light
Pin-hole

Interference filter

CCD Camera

Sample

Reference flat

Fig. 5: Experimental set-up

The light source is an incandescence lamp filtered by an interference filter (λ_0=650nm, $\Delta\lambda$=10nm). The interference filter drives the temporal light coherence and consequently the measurement depth on the sample. This illumination avoids all extraneous fringes induced with classical high coherence sources such as lasers.

This interferometer is conceived as a modular bench: by a simple lens change two configurations are available, high in-plane resolution or large field of view. We can analyse either very sharply (around 5µm) the micromirror structure inside a small field (typically 1mm) or the whole device with larger size (up to 40mm). For the high-resolution configuration, diffraction limit (N=4) is obtained In Fig. 6 is shown a fringe pattern on the tiltable mirror made in the Cronos foundry. Fringes are clearly seen on the 4µm-wide reflective coating on top of the torsion bar.
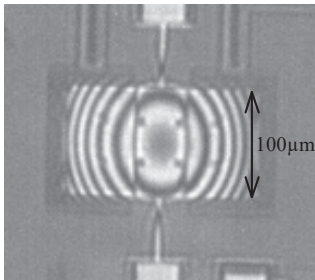

100µm

Fig. 6: Tiltable mirror made in Cronos foundry

Using interferometric techniques, we measure the wavefront phase $\Phi(x,y)$, which is directly related to the component shape $h(x,y)$ by Eq. (2) where λ_0 is the central wavelength.

$$\phi(x, y) = \frac{4\pi h(x, y)}{\lambda_0} \tag{2}$$

Our measurement techniques require a fine motion of the reference mirror. For this purpose, a piezo-electric stage (Polytec-PI P-752.1CD) in closed loop with a capacitive sensor (Fogale) is placed behind this mirror. The stage stroke is 15µm and the position is known with a sub-nanometre resolution. Two measurement methods are developed: phase-shifting interferometry for high out-of-plane resolution (few nanometres) and white-light interferometry to get large range (few microns) measurements. The former is implemented and the latter is still under development.

3.2. Phase-shifting interferometry (PSI)

Phase-shifting interferometry consists in moving the fringes step by step with the piezo stage. Eq. 3 defines the intensity signal Ii for the ith step. I_0 is the incident illumination; δ_i is the phase-step, and V the visibility of the fringes. The visibility depends on the different reflectivity factors, the spatial coherence and the temporal coherence. The movement of the component can also decrease the visibility, see paragraph 4.

$$I_i(x, y) = I_0(x, y)\big[1 + V(x, y)\cos\big(\phi(x, y) + \delta_i\big)\big] \tag{3}$$

We implemented the PSI algorithm developed by Hariharan [4]. The reference mirror is displaced in five positions δ_i defined in Eq. 4.

$$\delta_i = -\pi, -\frac{\pi}{2}, 0, \frac{\pi}{2}, \pi \tag{4}$$

The phase is then calculated with Eq. 5 and the contrast with Eq. 6.

$$\phi(x, y) = \tan^{-1}\left\lfloor \frac{2(I_2 - I_4)}{2I_3 - I_5 - I_1} \right\rfloor \tag{5}$$

$$V(x, y) = \frac{3\left[4(I_4 - I_2)^2 + (I_1 + I_5 - 2I_3)^2\right]^{1/2}}{2(I_1 + I_2 + 2I_3 + I_4 + I_5)} \quad (6)$$

The Hariharan algorithm is optimised for the phase measurement, even though the contrast measurements are sensible to noise. Error sources such as phase step error, air turbulence vibration or thermal drift are identified and minimized. The interferometer is mounted on a damped optical table and we are currently building a Plexiglas box to prevent air turbulence.
Since the phase is only known between 0 and 2π, the overall phase is unwrapped using a simple path-following algorithm.

The main characteristics of the bench are summarized in Table 1.

Table 1: Summary of the bench characteristics

	High resolution	Low resolution
Magnification	4X	0.25X
Horizontal resolution	5µm	100µm (centre) 250µm (edge)
Field of view	2.5mm	40mm
Vertical resolution	10 nm	20 nm
Vertical repeatability	<10nm	<10nm

3.3. Influence functions of OKO mirror

For WFC systems, the actuators stroke and the influence matrix are the main parameters of the deformable mirror. Influence matrix is the matrix giving a deformation vector for an excitation vector. It is calculated by concatenating the influence functions of each actuator. The influence function is the deformation of the mirror when a unit excitation (here square of the applied voltage) is applied on the actuator. Therefore with this influence matrix we can predict the shape of the deformable mirror for any excitation vector.
PSI technique has been used for the influence functions determination of the commercial OKO deformable mirror. The shape of the mirror without any voltage applied is shown in Fig. 7. Horizontal scales are pixels (1 pixel=30µm) and the vertical scale is nanometres. The static shape shows astigmatism of 650nm±10nm, in agreement with the data given by OKO [1].
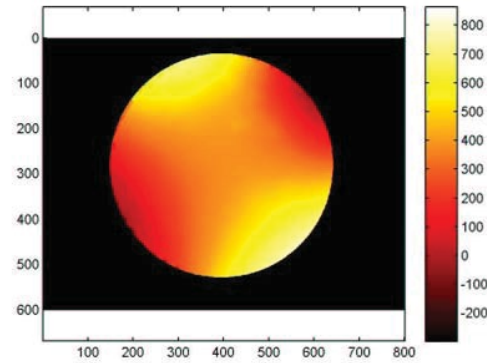

Fig. 7: Static shape of the OKO mirror

When the maximum voltage is applied on one electrode (Fig. 8), the influence function of this actuator (Fig. 9) is calculated by subtracting the shape of the mirror to its shape at rest (Fig. 7). The stroke of the actuator 1 is 370±10nm for 150 volts.
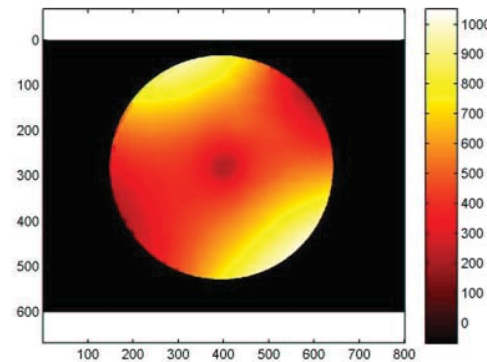

Fig. 8: 150 volts applied on electrode 1

According to Eq. 1, the membrane deformation is linear with the square of the applied voltage. The so-called influence function of actuator 1 is the result presented in Fig. 9 divided by 150².
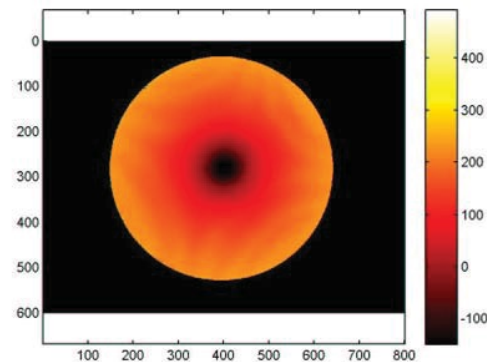

Fig. 9: Influence function of actuator 1

Using this procedure, all influence functions are determined and the influence matrix can be reconstructed.

3.4.   Results with Cronos components

PSI is limited at the measurement of sharp steps smaller than $\lambda/4$ because of the necessary phase unwrapping. This limitation is visible when print-through steps are present on the device, as in the case of the Cronos tiltable mirror.

Therefore "continuous zones" are selected on the component and the phase is unwrapped inside these zones. Finally the sharp steps (600nm high) are measured with a chromatic coding optical profilometer (STIL) and the different zones are gathered. In Fig. 10 is shown the shape of the tiltable mirror made by Cronos process. Horizontal scales are pixel (1pixel=2μm) and vertical scale is nanometres.
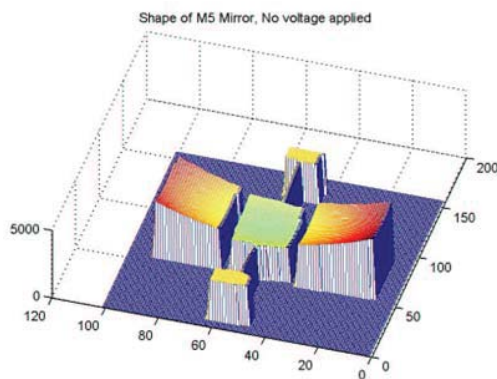

Fig. 10: Static shape of Cronos tiltable mirror

A peak-to-valley value of 2.2μm (steps included) and an arm deflection of 700 nm are measured. The curvature radius of the mirror is 3.0±0.3 mm due to the stresses introduced during the fabrication. This result shows that even for a claimed optimized process, high curvature values are still found on the devices. Future developments have to be made in order to minimize those effects.

Then different voltages are applied on the electrodes underneath and the difference is made with the static shape. The difference between the shape of the mirror with 19 volts applied on the left electrode and the shape at rest is shown in Fig. 11. Vertical scale is nanometres and horizontal scale is pixels (1pixel=2μm). The motion is a rotation movement (15±1 arc minutes) and a small piston effect (100±10 nm) due to the small width of the torsion bar. No deformation of the mobile plate surface is observed during motion.
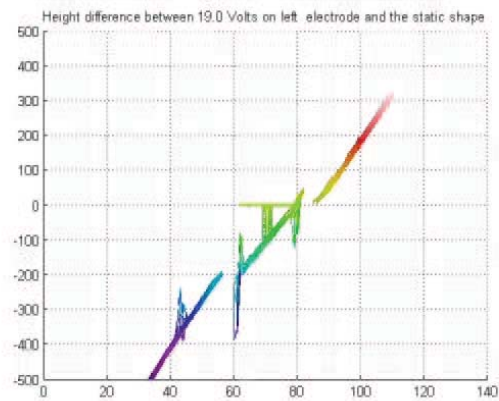

Fig. 11: Sum of rotation and piston movement

In order to measure a pure piston of the mobile plate, 23 volts are applied on both electrodes. Fig. 12 is the difference between the shape when actuated and the shape at rest. Vertical scale is nanometres and horizontal scales are pixels (1pixel=2μm). The motion is mainly a piston movement caused by the arms deflection (250±10nm). A limited deformation of the plate surface is also revealed: a small deflection effect in the direction left-right (70±10 nm left side and 30±10 nm right side) and a deflection in the direction of the arm (20±10 nm between the centre and the arm attachment).
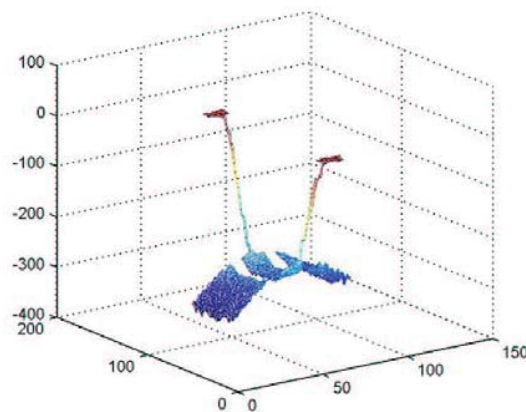

Fig. 12: Piston movement and mirror deformation

These results must be also considered as input data for simulations in order to design an optimized architecture of micro deformable mirror with improved performances.

4. QUANTITATIVE TIME-AVERAGED INTERFEROMETRY

4.1. Technique

Dynamic behaviour such as vibration modes or cut-off frequency of the device can be analysed by the contrast evolution while operating frequency is increasing. The movement of the component decreases the contrast of the fringes by time-averaging effect due to the CCD camera integration time. This diminution could easily be linked to the motion amplitude for one pixel [5]. This technique is known since 1970's as Electron Speckle-Pattern Interferometry (ESPI) [4].

Excitation of the component (Eq. 7) is done by applying a sinusoidal voltage (V_a) at frequency f_0 plus a bias (V_0) between the electrodes.

$$V(t) = V_0 + V_a \cos(2\pi f_0 t) \qquad (7)$$

Owing to Eq. 1, the displacement of the component is linear with $V(t)^2$. Eq. 8 defines the movement $h(t)$, which is decomposed in two harmonics. h_0 is the mean position, a_ω is the amplitude of the fundamental oscillation, $a_{2\omega}$ is the amplitude of the second harmonic and H is the frequency response of the component.

$$h(t) = h_0 + a_\omega \cos(2\pi f_0 t) + a_{2\omega} \cos(2\pi 2 f_0 t) \qquad (8)$$

Where

$$h_0 = H(0) * \left(V_0^2 + \frac{V_a^2}{2} \right)$$

$$a_\omega = H(\omega) * (2V_0 V_a) \text{ and } a_{2\omega} = H(2\omega) * \frac{V_a^2}{2}$$

In consequence, Eq. 3 defining the interferometric signal becomes Eq. 9. V is the visibility without excitation and J_0 is the first order Bessel function.

$$I_i = I_0 *$$
$$\left| 1 + V J_0\left(\frac{4\pi a_\omega}{\lambda_0}\right) J_0\left(\frac{4\pi a_{2\omega}}{\lambda_0}\right) \cos\left(\frac{4\pi h_0}{\lambda_0} + \delta_i\right) \right| \qquad (9)$$

With V_0 and Va such as $a_\omega >> a_{2\omega}$, the motion can be considered sinusoidal at frequency f_0, Eq. 9 becomes Eq. 10.

$$I_i = I_0 \left[1 + V J_0\left(\frac{4\pi a_\omega}{\lambda_0}\right) \cos\left(\frac{4\pi h_0}{\lambda_0} + \delta_i\right) \right] \qquad (10)$$

After calculation of the contrast by Eq. 6 for a given frequency and the contrast of the fringe pattern in the mean position, the ratio of these two contrast maps leads to the Bessel term. Using the bijective part of the Bessel function, i.e. a_ω inferior to $2.404 * \lambda_0/4\pi$, the motion amplitude a is obtained.

4.2. Results with OKO mirror

The OKO mirror is excited uniformly with a sinusoidal voltage (V_0 =55V and Va =2.2V) on its 37 electrodes. The condition $a_\omega >> a_{2\omega}$ is completed, and the movement of the membrane can be considered as sinusoidal.

In Fig. 13 a) is shown the interferogram of the OKO mirror in the mean position; Fig. 13 b) represents the interferogram when a sinusoidal voltage is applied. The contrast is clearly decreased, i.e. the amplitude a_ω is important, at the centre when the sinusoidal voltage is applied.
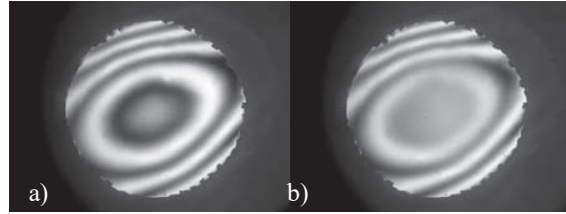

Fig. 13: Interferograms of OKO mirror at 1.2kHz
a) V_0 =55V and Va =0V   b) V_0 =55V and Va =2.2V

The frequency response (Fig. 14) of the OKO mirror has been measured on the [0, 2kHz] domain, which is the classical domain of WFC. This frequency response expressed in dB is $20\log(a_\omega)$ normalized by low-frequency response versus the logarithm of the frequency, and the experimental points are displayed with error bars. A resonance frequency is clearly visible around 1.2kHz. A theoretical second-order response is fitted on the experimental curve. Values of f_r =1170Hz and Q=2 are found for the second-order curve, where Q is the quality factor and f_r the resonance frequency. The valley observed at 1.1kHz could be explained by the fact that the first resonance frequency of the membrane is damped by an air cavity behind the membrane, according to OKO Company.
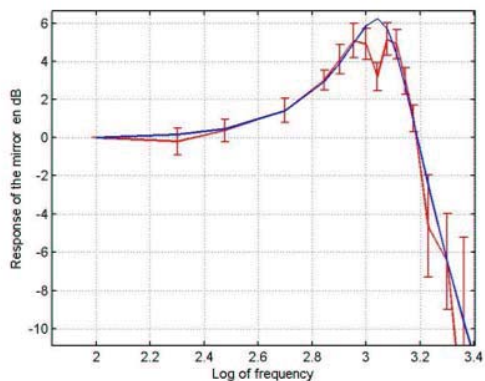
Fig. 14: Frequency response of OKO mirror

In Fig. 15 is shown the shape of this mode at 1kHz. Horizontal scales are pixels (1pixel=30μm) and vertical scale is nanometres. The ripples on the edge are residual errors during evaluation of the contrast.
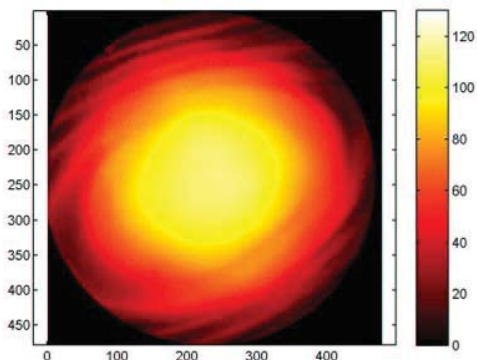

Fig. 15 : OKO vibration mode at 1 kHz

WFC loop must operate at frequencies below the resonance peak of the deformable mirrors. According to the results presented before, this mirror is well suited for WFC loop (such as for Adaptive Optics systems) up to 500 Hz, in agreement with OKO data.

4.3. Results on Cronos device

A sinusoidal signal (V_0 =14V and Va=3V) at different frequencies is applied on the right electrode. V_0 and Va are optimized for having the optimal deflection.
The frequency response (Fig. 16) of this device is close to a second order system. The resonant frequency is 31±2 kHz and the damping is large. This frequency response is expressed in dB. Experimental points are displayed with error bars and a theoretical curve of a second-order system with f_r=31kHz and Q=0.94 is fitted. The vibration mode of this device is a sum of rotation mode and piston mode.

In order to obtain a pure piston movement, as observed in paragraph 3.4, an identical voltage (V_0 =16.22V and Va=5.77V) is applied on both electrodes. Experimental points are displayed with error bars on Fig. 16 and a theoretical curve of a second-order system with f_r=63kHz and Q=0.8 is fitted. The piston cut-off frequency is higher than the rotation cut-off. This result was predictable because of the existence of piston effect even after the cut-off frequency for the rotation movement.
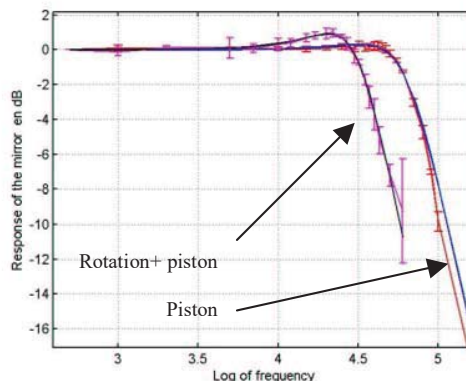

Fig. 16: Frequency response of Cronos mirror

In Fig. 17 is shown the displacement map at 45kHz. Horizontal scales are pixels (1pixel=2μm) and vertical scale is nanometres. We can notice that the amplitude is larger (25nm approximately) at the left and right extremity than in the centre. This is due to the deformation of the plate seen in paragraph 3.4. This deformation effect is still present after the cut-off frequency of the piston mode. This means the cut-off frequency of this additional mode is higher than 80kHz.
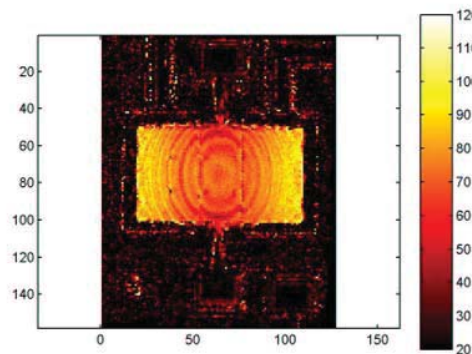

Fig. 17: Piston mode at 45 kHz

Dynamic study of this mirror shows very high cut-off frequency. Therefore time response of micro deformable mirror based on this technology should be in agreement with the WFC requirements.

5. PERSPECTIVES

Using the modularity of the bench, several improvements are planned in a near future for increasing its measurement capabilities.

5.1. White-Light interferometry (WLI)

In order to remove the 2π ambiguity introduced by interferometry, we are developing white light interferometry. The position of the component can be known without ambiguity by scanning along the z-axis and finding the maximum of coherence (white fringe) [6]. White-light phase shifting interferometry (WLPSI), combining WLI and PSI should provide high-resolution vertical measurements with large range [7].

5.2. Two-wavelength phase-shifting interferometry (TWPSI)

Two-wavelength PSI should increase the range of PSI measurements without loosing its accuracy [8] and overcome the coherence length dependence of WLI.

5.3. Stroboscopic illumination

Using a stroboscopic illumination for freezing fringes during a periodic motion, dynamic behaviour of the component could be analysed without sign ambiguity, amplitude limitation and with a better resolution [9].

5.4. Materials characterization

Easy and high-precision measurement of material properties is essential for optimizing MEMS design and determining process control [10]. By using interferometry to measure the full deflection curves of simple beams, values for material parameters such as strain gradient, Young's modulus and residual stress could be extracted by comparison with a model.

6. CONCLUSION

Since MOEMS will be used in future WFC systems, a high-resolution Twyman-Green interferometer has been developed for micro deformable mirror characterization. Measurements have been done on a commercial OKO deformable mirror as well as on in-house designed devices. Static characterization (surface quality, deformation) is realized by phase-shifting interferometry, and dynamic characterization (frequency response) by quantitative time-averaged interferometry. From these measurements, the influence functions of the OKO mirror are determined and we will design more accurately our micro deformable mirrors through comparison with simulation.

REFERENCE

1. G. Vdovin et al., "Flexible mirror micromachined in silicon", *Applied Optics,* 34, p.2968, (1995)
2. T. Bifano et al., "Continuous-membrane surface-micromachined silicon deformable mirror", O*pt. Eng., 9(4),* 2000
3. F. Zamkotsian et al., "Micro-deformable mirror for next generation adaptive optical systems", *SPIE "Astronomical Telescopes and Instrumentation 2002"*, Hawaii, USA, 2002
4. D. Malacara et al., *Optical Shop Testing,* Second Edition*,* John Wiley & Sons, 1992
5. S. Petitgrand et al., "Quantitative time-averaged microscopic interferometry for micromechanical device vibration mode characterization", *Pro. Microsystem Engineering: Metrology and Inspection II,* 2001
6. K. Larkin, "Efficient nonlinear algorithm for envelope detection in white light interferometry", *J. Opt. Soc. Am. A.,* 13, p.832, (1996)
7. A. Harasaki et al., "Improved vertical-scanning interferometry", *Applied Optics.,* 39, p.2107, (2000)
8. Y. -Y. Cheng and J.C. Wyant, "Two-Wavelength Phase Shifting Interferometry", *Applied Optics,* 23, p.4539, (1984)
9. M. Hart et al., "Stroboscopic interferometer system for dynamic MEMS characterization", *Journal of microelectromechanical systems, 9(4),* 2000
10. B. Jensen et al., "IMaP: Interferometry for materials property evaluation in MEMS", *Pro. MSM'99*, p.206, 1999